

Dipole–dipole interaction induced phases in hydrogen-bonded squaric acid crystal

Vikas Vijigiri^{1,2} and Saptarshi Mandal^{1,2,3} 

¹ Institute of Physics, Bhubaneswar-751005, Orissa, India

² Homi Bhabha National Institute, Mumbai-400 094, Maharashtra, India

E-mail: vikasvikki@iopb.res.in and saptarshi@iopb.res.in

Received 11 November 2019, revised 27 January 2020

Accepted for publication 2 March 2020

Published 15 April 2020



Abstract

We study the finite-temperature phase diagram of proton ordering of a quasi-two dimensional hydrogen-bonded system, namely the squaric acid crystal ($\text{H}_2\text{C}_4\text{O}_4$) using quantum Monte Carlo. We take into account the four-spin plaquette interaction at the zeroth order followed by next nearest neighbor Ising interaction within a plaquette, dipole–dipole interaction and an external transverse magnetic field respectively. Using an improvised loop algorithm within the stochastic series expansion (SSE) quantum Monte Carlo method, we find two distinct phases as we increase the temperature and magnetic-field. One of the phase is the Π_f , the phase with long range ferroelectric order and the other being an intermediate state with strong local correlations, i.e., a quantum liquid-like state Π_{ql} . The transition to Π_f shows a very small anomalous peak in the specific heat with strong dependence of critical temperature on the strength of dipole–dipole interaction. The presence of the small peak is attributed to the absence of macroscopic degeneracy in the presence of dipole–dipole interaction and re-entrance of such degeneracy to some extent at small temperature. The work also discusses an intricate connection of quantum fluctuation and thermal fluctuation in the presence of competing interaction with entropic effects.

Keywords: squaric acid, ferroelectric phase, ice rule, quantum paramagnetic state

(Some figures may appear in colour only in the online journal)

1. Introduction

The observation of finite temperature phase transition in condensed matter system is a common phenomena since unknown past. We know how various types of phase transition phenomenon, for example, the metal to superconductor phase transition or solid to liquid to vapor transition or the structural and magnetic transition are brought in due to the changes of temperature. As the temperature changes, the interactions between constituent particles are renormalized or tuned so that new phases of matters appear. The interplay of competing interactions, quantum as well as the thermal fluctuation play key roles in such events. In this article we will be discussing the combined effect of finite temperature, competing interactions as well as magnetic field in a well known material known as squaric acid, commonly represented as $\text{H}_2(\text{SQ})_4$ where SQ

generally represent a structural unit (e.g.: C_4O_4). This particular material had drawn the attention of condensed matter physicists (theory and experiment alike) over more than half a century [1–8]. The material is very intriguing, as the primary interaction is governed by the hydrogen bonds and the associated proton dynamics. The material is a layered three dimensional one where each two dimensional layer is made of square lattice like structure [9] with each square containing a unit of SQ. Each of them are held together by hydrogen bonds which is mediated by protons. An individual proton undergoes quantum tunneling between double well potential [1, 2] as found from the isotope effect study of this material. The proton motion is conveniently modelled as a quantum spin (spin 1/2) model.

H_2SQ is very similar to water ice system, where the local constraint in the form of ‘ice-rules’ dictating the proton ordering restricts the ground state to have configurations where in

³ Author to whom any correspondence should be addressed.

each molecule has exactly four hydrogen-bonds with two protons being near to C_4O_4 unit and the other two being at far [10, 14–16]. Apart from the proton dynamics and the interactions between them, the material possesses dipole–dipole interactions which is evident from the fact that it undergoes a paraelectric to ferroelectric phase transition [9]. These systems are of particular interest because not only that these systems exhibit some of the peculiar properties: showing no signs of phase transition, i.e., they tend to be disordered down to few milli Kelvins, there is frustration or competition leading to ‘residual’ or ‘zero-point entropy’ [10]. In some cases, strong fluctuations with high degree of entanglement between the ice-rule configurations may lead to exotic phases like quantum-spin liquid [17–21]. Long back, this ‘ice-rule’ constraint and the movement of protons on H_2SQ were mapped into suitable vertex model or quantum pseudo spin model [24–26] to understand the anti-ferroelectric properties. Further, the thermal motion of an SQ-unit in a squaric acid system is strongly coupled with the proton movements. This motivated the study of interaction of phonons with pseudo-spins [27–29]. Though these pioneering works had successfully examined some key features of the system, many of the theoretical methods were mostly limited at the mean-field level without consideration of the effect of geometrical frustration rigorously. For example, quantum fluctuation along with the entropic effects, which is presumably important for understanding the quantum paraelectricity under pressure has not been seriously considered so far.

As already mentioned, hydrogen-bonded (HB) crystals are also known for their ferroelectric polarizability due to certain proton ordering (e.g.: KH_2PO_4 , H_2SQ). There have been ample studies regarding the electronic polarization emerging from certain ordering of proton configurations in the system with emphasis on both the fundamental physics and the application to electronic devices [22, 23]. Apart from these, one of the interesting feature of H_2SQ is that, in general, the external pressure increases the tunneling rate of protons between the two potential minima, which reduces local polarizations, and consequently, suppresses the ferro-electricity. Indeed, in H_2SQ , T_c is suppressed with increasing pressure. A peculiar intermediate state, however, appears before the polarization is lost in each molecule: the macroscopic polarization vanishes while the polarization in each molecule is retained [11]. Consequently, a quantum para-electric state is realized in the low-temperature limit. Thus the material presents an unique test bed where the effect of external pressure as well as temperature could be investigated on the proton dynamics so that a number of interesting and competing aspect can be observed in a single study. The model Hamiltonian we consider here is given in (2.1). The model Hamiltonian at zeroth order consists of a four-spin plaquette interaction with a strength J_0 . When the Hamiltonian is studied in the presence of a magnetic field characterized by the parameter K , the system shows a confinement–deconfinement phase transition. The model also includes a next-nearest-neighbor Ising-like interaction with a strength J_1 and a dipole–dipole interaction $J_2 < J_1$. Usually, the presence of J_2 causes the ferro-electricity of these

materials. The model was shown to exhibit both confinement–deconfinement transition (CDT) and ferroelectric quantum phase transition (FT) for an appropriate set of parameters of the model Hamiltonian. However, in the present paper we study the finite temperature (incorporated with magnetic-field) properties of each of these phases. In the presence of intra-molecular coupling term J_1 , we identify a smooth crossover to para-electric phase from a globally disordered dipole phase. In the presence of J_2 , the system gets ferro-electrically ordered at low temperatures and with the increase of field strength K , the ferroelectric phase undergoes to a para-electric phase which also undergoes a finite temperature second order phase transition to a conventional para-electric phase. We then numerically chart out the phase diagram in the T – K plane. In particular to this model Hamiltonian we treat the effect of geometrical frustration rigorously unlike the earlier studies, which were limited at the mean-field level. We use an unbiased stochastic series expansion (SSE) quantum Monte Carlo (QMC) technique to take into account the quantum fluctuation under the entropic effects (arising from the ice-rules), which is presumably important for understanding the quantum para-electricity under pressure. Our study is also important in a way that for such an interacting four-spin Hamiltonian, we have been able to obtain the phase diagram successfully with appropriate quantum Monte Carlo scheme.

The organization of this paper is as follows. In section 2, we introduce the effective model Hamiltonian and methods to analysis it. After introducing the pseudo-spin model in section 3, we briefly discuss the implementation of SSE QMC method used for our Hamiltonian. We then explain the order parameter that has been calculated in our analysis. The results obtained from our SSE QMC simulation have been presented in detail in section 4. In section 5, we discuss our results in a broader perspective including a qualitative comparison with the relevant earlier experimental and theoretical studies.

2. Model and method

2.1. Pseudo-spin model

In this section we introduce the full Hamiltonian that we consider. The terms that we include have already been considered before as well [12, 13] and is given below

$$H = -J_0 \sum_{\langle ijkl \rangle} A_{\square} + J_1 \sum_{\langle ij \rangle} B_{\square} - J_2 \sum_{\langle AB \rangle} \vec{P}_A \cdot \vec{P}_B - K \sum_i \sigma_i^x \quad (2.1)$$

where $A_{\square} = \sigma_1^z \sigma_2^z \sigma_3^z \sigma_4^z$, the indices i, j, k, l represent the four spins on the edges of a plaquette, $B_{\square} = (\sigma_1^z \sigma_3^z + \sigma_2^z \sigma_4^z)$, the indices i, j here represent spins opposite to each other on a plaquette of the square lattice, and $P_{A,B}^x = \pm \frac{1}{4}(\sigma_1^z + \sigma_2^z - \sigma_3^z - \sigma_4^z)$, $P_{A,B}^y = \pm \frac{1}{4}(\sigma_1^z + \sigma_4^z - \sigma_2^z - \sigma_3^z)$ are the dipole-moment vectors for A, B sub-plaquettes as illustrated in figure 1.

The parameter space of the Hamiltonian H is three dimensional with J_0 being the largest followed by K , J_1 , and J_2 in magnitude. J_0 (>0) gives rise to \mathbb{Z}_2 gauge invariance and the intra-molecular coupling term J_1 gives rise to the restricted ice rules implying that only those states with ice rules

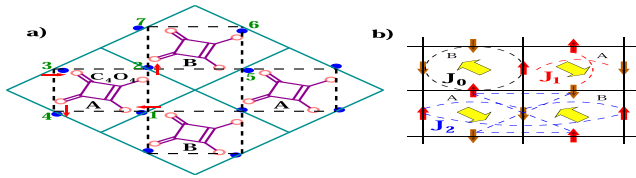


Figure 1. (a) Squaric acid network system, the blue dots represent the hydrogen atoms and the small pink circles represent the oxygen atoms of the molecule H_2SQ forming a quasi-two dimension configuration of hydrogen-bonded network, here SQ being the C_4O_4 unit is shown. The dashed brown lines show the physical lattice and the solid cyan lines form the lattice on which the model is built on. The indices shown represent the corresponding spins as shown in in equation (2.1). (b) We present one of the configuration of the ferroelectric ordering, the yellow arrow indicate the polarization axis. The dotted color lines are drawn to indicate bonds/plaquette for each interaction of the Hamiltonian, J_0 (black), J_1 (red), J_2 (blue).

having finite dipole moment are allowed. The presence of four-spin interactions signified by the coupling J_0 stems from the fact that for a real H_2SQ molecule, the energy of a given molecule does depend on the relative position of the four hydrogen ions it shares with neighboring molecules [3]. This is particularly important because though at zeroth order the hydrogen ions are assumed to be tunneling in a quantum double well potential and thus an Ising-like two-spin interaction could also be a possible candidate for dynamics at zeroth order. However, as the height of the potential well is not significantly large, a more general four-spin interaction is more suitable [1]. The second term of the Hamiltonian appears naturally from an approximated, possible two-spin interaction for a plaquette. Remember that for a plaquette there can be four nearest-neighbor Ising-like interactions and two Ising-like interactions across the diagonal links. The energy scale of these two types are different and the previous four types of Ising exchange interactions are an approximate representation of the general four-spin interaction represented by J_0 . Since the ground states results in finite dipole moment in each square plaquette, a more general Hamiltonian would also have a dipole–dipole interaction term J_2 . The presence of dipole–dipole interactions is also inevitable from the fact that without their presence the observed ferroelectric transition would not be possible as argued in reference [1]. The physical origin of dipole–dipole interactions arises naturally when the local ground-state or zeroth-order electrostatic energy is disturbed by the vibrational modes of the ‘SQ’ molecules thus giving rise to nearest-neighbor dipole–dipole interactions.

2.2. Stochastic series expansion quantum Monte Carlo method

With the rapidly emerging focus of quantum Monte Carlo methods (QMC) for an unbiased calculations the hunt for an efficient cluster algorithms is on as far as stochastic series expansion (SSE) QMC method is concerned. The last few decades has very limited success in developing efficient algorithms at finite temperature especially for systems with frustration or for systems with macroscopic degeneracy. Earlier methods relied on constructing the clusters based on a ‘link-decomposition’ of Hamiltonian found

to be inefficient, despite being tried in various forms by constructing the clusters along τ -dimension (imaginary-time). Nevertheless, here we use a variant of a recently developed micro-canonical cluster algorithm (quantum cluster update) where it uses the plaquette decomposition of the Hamiltonian within the framework of stochastic series expansion (SSE) pioneered by Sandvik and others [30–38]. Clusters are constructed based on a plaquette percolation process with the notion of ‘premarked motifs’ which act as a flag in determining the way in which it connects the legs of all diagonal plaquette operators ‘living on’ various planes of imaginary-time direction. Once all clusters are constructed, each can be independently flipped with probability 1/2 within a Swendsen–Wang type implementation. Here in the present study, we have employed and improvised an algorithm within the stochastic series expansion Monte Carlo method [37]. Readers interested in the details regarding the efficiency and performance of the algorithm compared to percolation based algorithm can find here [37] for an ‘odd’ Ising gauge Hamiltonian with anti-ferromagnetic Ising exchange term. The major difference in the design of the algorithm is that the choice of premarked motifs differ for each systems with complicated interactions or frustration, where an intuition or little prior knowledge of the equilibrium ensemble is a bonus for improving the algorithm further, this is also where we had implemented our idea to investigate the Hamiltonian we considered.

Since there are three distinct regions corresponding to three different parameters J_0, J_1, J_2 , we thus identify different premarked motifs choice as shown in figure 2. In figure 2(a), we provide the cartoon picture of pre-marked motif for a general plaquette four body interaction signified by finite J_0 and $J_{1,2} = 0$. In the figure 2(a), we show a privileged single site premarked motifs. It is easy to find that there are four such choices corresponding to four sites in a given plaquette. In figures 2(b) and (c), we represent in pink shaded region, the sites whose spins are to be flipped. They all corresponds to the single site premarked motif described in figures 2(a) and (d), we represents the choice having two sites as the preferred premarked motifs. There are two such choices.

For $J_1 \neq 0, J_2 = 0$, the only choice of premarked motifs are shown in figure 2(d) where two frustrated bonds (only those with one parallel to other) are required to be on each plaquette which corresponds to eigenvalue $4J_0 + 4J_1$, while configurations with four or zero frustrated bonds have eigen-value zero and hence corresponding plaquette operators do not appear in the operator string. Our choice of motif in the $J_2 \neq 0$ case also consists of two privileged diagonal sites among the four that make up a spatial plaquette as in figure 2(d). Thus each spatial plaquette has two distinct possible motifs. The motif on a given spatial plaquette determines the cluster decomposition of plaquette operators at that location in the following way: if only one frustrated bond touches the two privileged site, the four legs corresponding to these two sites are assigned to a *a priori* different cluster, and the other four legs make up the other cluster. If the privileged site is touched by two or zero frustrated bonds, then the four legs corresponding to the privileged site and its diagonally opposite site are assigned to one

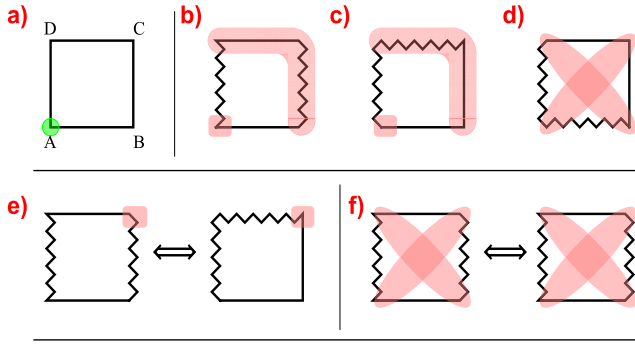


Figure 2. Various choices of cluster decomposition rule for premarked motifs are shown in (a)–(d). In (e) and (f) we show the distributions of parallel and anti-parallel bonds corresponding to the above choices. The zigzag lines indicate the bonds consisting pair of anti-parallel spins, the frustrated bonds and unfrustrated bonds correspond to solid lines.

cluster, and the other four legs are assigned to a different cluster (which could in principle merge with the other cluster at a future step in the cluster construction).

We observe that in the case of $J_1 \neq 0$ there is no apparent spin-freezing thus making the algorithm much more efficient in this regime. However, despite improvising the sophisticated algorithm to work in the case $J_1 \neq 0$, we see some apparent spin freezing at low temperatures and hence to avoid that we also invoke the replica exchange method with temperatures ranging from 0.05 to 1.0. We use system sizes varying from $L = 24$ to 32 ($N = 2L^2$) with a standard 1×10^7 iterations for equilibration and 1×10^7 for measurements. Results are divided into six bins to estimate statistical errors by the variance among the bins.

3. Physical quantities

In view of the wide scope of our model which might host different phases dependent on the relative magnitude of the model parameter and temperature as well, we introduce the relevant parameters in detail. This will help us to identify each phases as well as to distinguish from each other without ambiguity. At very high temperature $T > J_i$, one generally expects a para-electric phase where the dipole moments associated with each plaquettes are disordered. The para-electric to ferroelectric phase transition (due to dipole–dipole interaction term J_2) as we lower the temperature is characterized by the order parameter P which is nothing but the electronic polarization and the associated susceptibility χ_P . They are defined as below.

$$P = \frac{1}{N} [|S(0, \pi)|^2 + |S(\pi, 0)|^2]^{1/2} \quad (3.1)$$

$$\frac{\chi_P}{N} = \beta [\langle p^2 \rangle - \langle P \rangle^2] \quad (3.2)$$

where $S(\mathbf{k})$ is the static spin-structure factor given by

$$S(\mathbf{k}) = \frac{1}{N} \sum_{i,j} S_i^z S_j^z \exp(-\mathbf{k} \cdot \mathbf{r}_{ij}) \quad (3.3)$$

To locate the critical temperature associated with this para-electric to ferroelectric phase transition, we use the

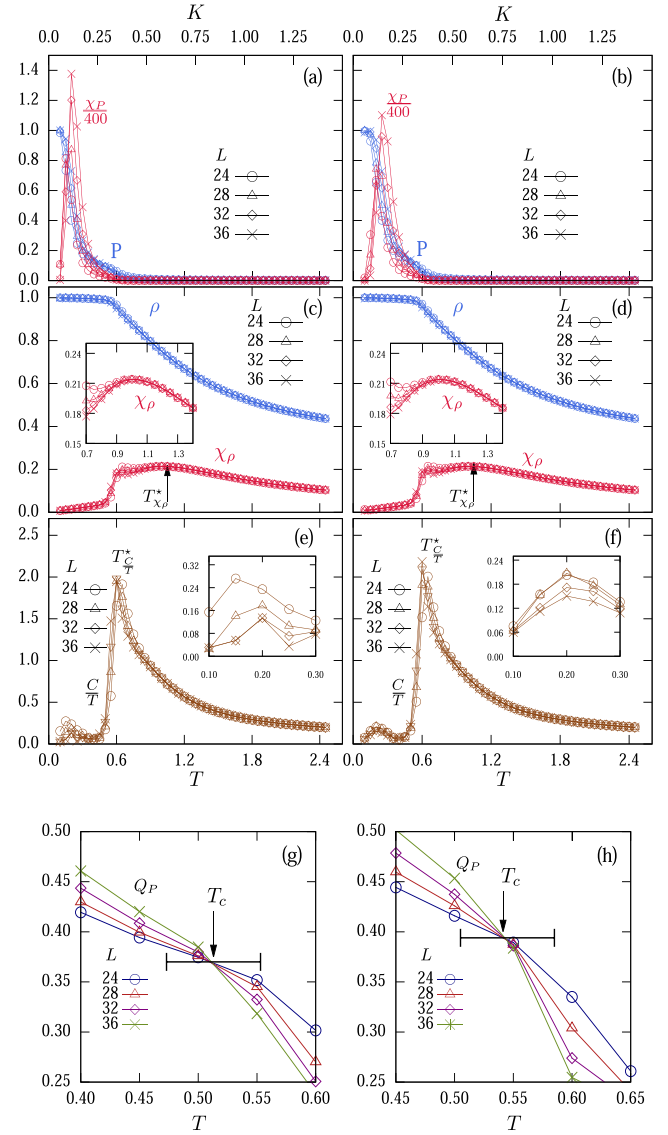


Figure 3. In panel (a) and (b) the red points and the blue points show the plot for χ_P and P . Similarly in (c) and (d), we present ρ and χ_ρ by red and blue points respectively. In (e) and (f), specific heat divided by temperature (C/T) has been shown. Binder parameter has been shown in panel (g) and (h). In all the plot, various different points denotes different system size as shown. All the results are calculated along the contour $K/T = \tan(\theta)$ where $\theta = \pi/6$. For detail description of the above, we refer section 4. The parameter values used in the figures are $J_0 = 1.0, J_1 = 0.5$ with $J_2 = 0.020$ for left panel and $J_2 = 0.024$ for right panel.

Binder cumulant analysis, where the binder parameter Q_P is defined as [40]

$$Q_P = \left(1 - \frac{\langle P^4 \rangle}{8 \langle P^2 \rangle^2} \right) \quad (3.4)$$

Apart from the presence of para-electric and ferroelectric phases, at very low temperature and for small values of J_2 (the strength of dipole–dipole interaction), the ground state is dominated by states determined by J_0 and J_1 . In this situation, the ground state manifold is dictated by the states which satisfy the ‘ice rule’. In true sense this is a quantum liquid states. To distinguish this state from the usual para-electric states, one needs to define an order parameter which can successfully establish the presence of this state and differentiate it from usual

para-electric phase and ferroelectric phase. To this end, we define the parameter ρ which detects the ice-rule state, i.e, the partially disordered locally-correlated liquid-like para-electric phase,

$$\rho = \frac{1}{N} \sum_p I(p) \quad (3.5)$$

where $I(p) \rightarrow 1$, if the given plaquette p is in one of the local four-fold degenerate ice-rule state and $I(p) \rightarrow -1/3$ otherwise. To further corroborate the results of phase transition and crossover we also calculate the susceptibility corresponding to ρ by calculating their fluctuations as given by,

$$\frac{\chi_\rho}{N} = \beta [\langle \rho^2 \rangle - \langle \rho \rangle^2], \quad (3.6)$$

where the crossover from the disordered but correlated dipoles into a para-electric phase can as well be detected in the specific heat measurements as shown in figure 3.

4. Results

We know from the earlier studies [12, 13] that presence of dipole–dipole interaction (the J_2 term in the Hamiltonian in equation (2.1) induces a ferroelectric order. In the absence of J_2 , the ground state is highly degenerate. The degeneracy for $J_1 = 0$ is exponential though with J_1 it is proportional to the peripheral size of the system. On the other hand the global ferroelectric order is four fold degenerate. Thus we see that the effect of temperature on the system might be very intricate due to the energy cost for low energy excitations due to competing interactions as well as due to degeneracy of the ground state manifold for each parameters. This actually necessitates to examine the order parameter P and ρ both. Interestingly we find that they does not follow each other as we increase the temperature. Correspondingly, the susceptibility also shows contrasting behavior. We first discuss the temperature dependence of P and ρ followed by the corresponding susceptibility.

4.1. Temperature dependence of P and ρ

The general behavior as evident from the QMC simulation suggests that as we turn on the temperature the ferroelectric order parameter denoted by P sharply decreases for a very small value of temperature. However this decrease seems to be a two steps process. We call the first phase of decrease of P as the quantum liquid states and the higher temperature counterpart as an usual para electric phase. The P shows a shoulder like hump at the transition from quantum liquid like states to para electric states. In figures 3(a) and (b), we have shown the variation of P in blue points for $J_0 = 1.0, J_1 = 0.5, J_2 = 0.020, 0.024$. The presence of quantum liquid like states is apparent from the temperature variation of ρ as presented in blue points in figures 3(c) and (d). We clearly observe that ρ is almost constant throughout this quantum liquid like state and decreases monotonically when the system yields to para-electric state. Thus the order parameter P and ρ suggest that as we increase the temperature from zero, the system starts from ferroelectric phase, moves to an intermediate quantum-liquid

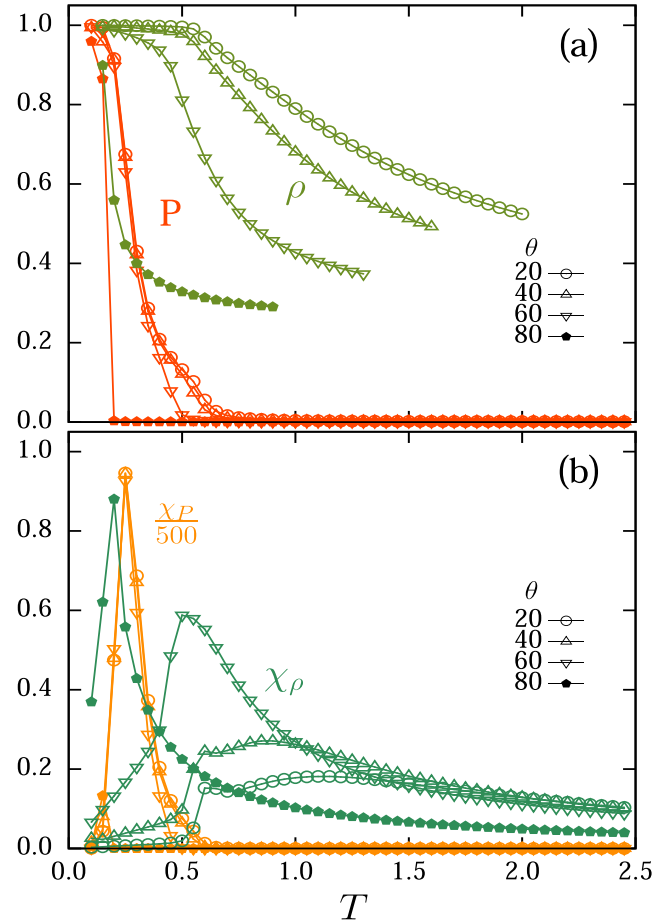


Figure 4. In the upper panel we show temperature dependence of order parameter and ice-rule parameter ρ by the orange and green points respectively. The corresponding susceptibility have been plotted in the lower panel with the same color convention as the upper plane. Note that in the above 2D plot each graph denotes a specific line in the T - K plane. Each line is represented by the corresponding slope of the line θ . For the details of the plot kindly refer to the text in section 4.

like state and finally reaches to a para-electric phase. In the upper panel of figure 4 we have shown by orange and green points more plots for the behavior of P and ρ respectively for various values of θ in T - K plane. It shows that for large values of θ , P and ρ decreases more rapidly than the small values of θ . This indicates that the pressure and temperature has opposite effect in the system. The pressure denoted by K tends to stabilize the ferromagnetic and the intermediate quantum liquid like state.

4.2. Susceptibility χ_P and χ_ρ and specific heat C/T

The susceptibility obtained due to P is shown in figures 3(a) and (b) by red points which shows a jump at the transition from ferroelectric phase to quantum liquid-like states. This suggests that ferro-electricity is almost destroyed at this transition. However the susceptibility corresponding to ρ , i.e. χ_ρ shows a very interesting feature. Initially it is almost zero, increases very slowly until the temperature reaches near to the transition from quantum liquid like states to the para-electric states. At this transition the χ_ρ jumps at a higher value and

remain almost constant up to a certain temperature which we call T_p and after this, χ_ρ decreases monotonically. The specific heat at very large temperature shows monotonically decreasing behavior characteristic to usual para-electric phase but at low temperature it shows two peaks of different magnitude as denoted in figures 3(e) and (f). The largest peak appears at the transition of quantum liquid like state and we denote this temperature by $T_{C/T}^*$. However, the sharp nature of the peak indicates a possible order–disorder phenomenon where the degeneracy seems to be uplifted to some extent. Below this temperature specific heat shows another small peak at where the P starts to decrease from initial constant value for small T . The peak height of this smaller one tends to decrease with increase of system size as denoted in the inset of figure 3. In the lower panel figure 4 we have shown the behavior of χ_P and χ_ρ respectively for various values of θ in T – K plane in orange and green plots respectively. It shows that for large values of θ , P and ρ has a more sharper peaks and also they decrease more rapidly compared to the small values of θ . It suggests that the stability of the intermediate liquid like state is enhanced by increasing the K/T ratio. This may be attributed to the fact that increase of K results into enhancing the bandwidth of the system resulting into decreasing the thermal effect.

4.3. Binder cumulant and critical temperature

In the foregoing discussion we have already introduced the two critical temperature. The largest one is the $T_{\chi_\rho}^*$ which is signified by the step like jump from almost zero values of χ_ρ to a higher value. Below this temperature we observed another critical temperature signified by the largest jump in the specific heat at the transition to para-electric phase from the quantum liquid-like state. This temperature is denoted by $T_{C/T}^*$. Our analysis for the Binder cumulant as shown in the figure 3 shows that the actual phase transition is very near to the $T_{C/T}^*$ and we denote this temperature as T_c . As for as our numerical results and analysis are concerned, $T_c = 0.56(47)$ and $0.56(03)$ for $J_2 = 0.020$ and 0.030 respectively. The corresponding $T_{C/T}^*$ is obtained as $0.060(03)$ and $0.61(40)$ respectively.

4.4. Phase diagram

The numerical results presented above suggest the presence of three phases as we increase the temperature. The first one is ferroelectric phase which survives for very small temperature and extends up to T_c as obtained from Binder cumulant. We call this phase as Π_f . The jump in the specific heat signified by $T_{C/T}$ is little higher than the T_c . Above the T_c there is a presence of a complex quantum liquid like state which extends up to some critical temperature $T_{\chi_\rho}^*$. This phase is very intriguing as long as the behavior of order parameter is concerned and we call this phase as Π_{ql} . After $T_{\chi_\rho}^*$, the normal para electric phase develops with no residual quantum correlation between the dipole moments. The above three critical temperatures defined above depend the values of J 's and the K . It is instructive to present above three phases in a contour plot in T – K plane and this is presented in figure 5. The results are shown for different J_2 strengths in the T – K

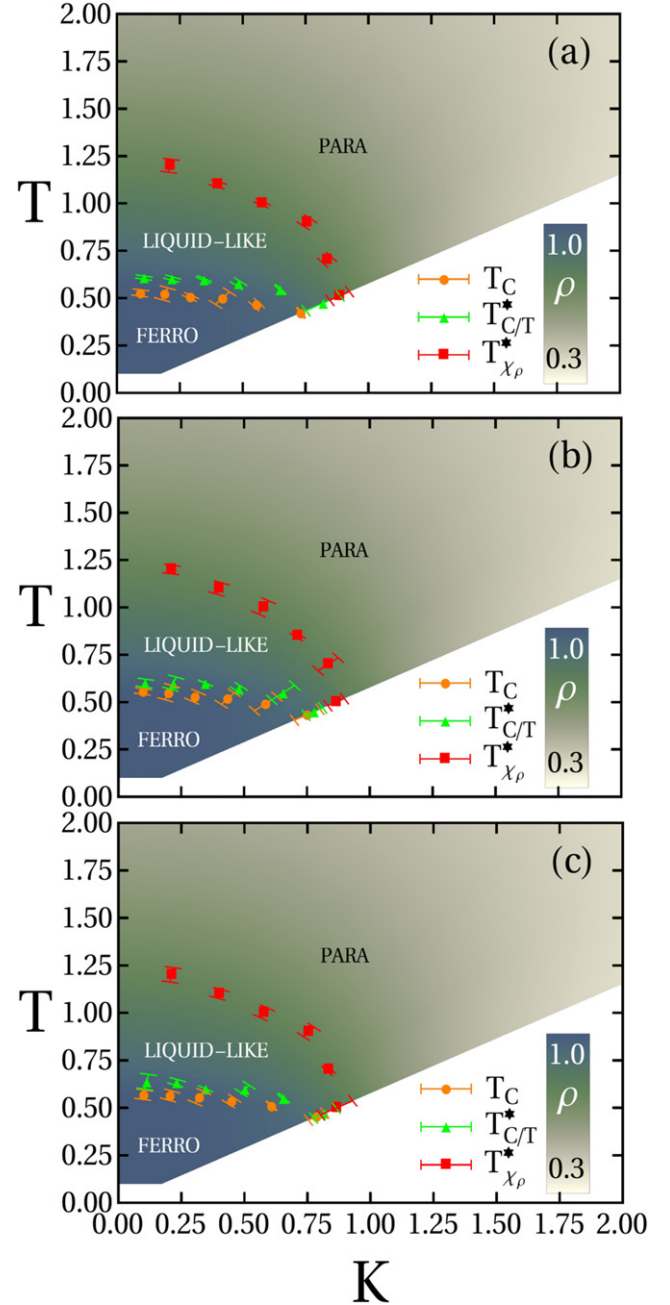


Figure 5. Phase diagram showing the critical and crossover points, the figures (a)–(c) correspond to the values $J_2 = 0.020$, $J_2 = 0.024$, $J_2 = 0.028$ respectively. The orange dots indicate the critical points for ferro to liquid like transition obtained from the binder analysis, green triangles indicate the cross over points $T_{C/T}^*$ obtained from the C/T curve, while the red squares indicate the $T_{\chi_\rho}^*$ obtained from χ_ρ .

plane. For the case where $J_2 = 0$ the system shows a crossover transition from quasi macroscopic degenerate liquid-like state to a completely disordered state, with the crossover temperatures shifting to higher temperatures with J_1 as expected. However even for J_2 very small, the system orders ferro-electrically (the region below T_c , orange circles), the region between the T_c and $T_{\chi_\rho}^*$ belongs to the liquid-like state.

It is interesting to note that the scaling behavior of the critical boundary shows unique characteristics, the boundary does not extend into the liquid-like region rapidly but

rather slowly indicating that the dependence of T_c with J_2 is complex with lower dynamic exponent than the model having only two body interactions [39]. Another aspect is that the ratio of thermal energy (T_c) to that of J_2 is also less. We believe that the colossal enhancement of T_c with J_2 is related to the lifting of quasi macroscopic degeneracy. The above finding could be confirmed by experiment in conjunction with a first-principle study yielding an estimation of the parameter of the model Hamiltonian. It is interesting to note that all the phase transitions that we observe is not of first order but rather like second order specially the transition from Π_f to Π_{ql} . On the other hand the transition from Π_{ql} to Π_p is a smooth crossover. The phase Π_{ql} and Π_f suggests quite an interesting behavior of ρ and C/T . Let us begin with Π_f first. At $T = 0$, the system is in ferroelectric state with global ground state degeneracy of four. As we increase the temperature, the ferroelectric order parameter P decreases rapidly but ρ remains constant and in addition we observe a small peak in C/T . This suggests that the global ferroelectric order reduces into domain of ferroelectric clusters and also includes the presence of other states not contributing to P but consistent with ice rules. The possibility of presence of these additional states explains the small peaks in C/T which also decreases as we increase the system size. As far as the phase Π_{ql} is concerned, we observe the steady decrease of the ice rule order parameter ρ which suggests that the excitations now includes the non-ice rule states as expected. However the quantum correlation is not lost completely until the critical temperature $T_{\chi\rho}$ is reached.

5. Discussion

We have considered a model where at zeroth order there is a four-spin Ising gauge like interaction of protons in the pseudo-spin formalism. Earlier results on the model showed that the system hosts a deconfined phase for $J_2 = 0$ [12] at zero temperature. We use the model here to extend the phase diagram along the finite temperature axis. Our results show an ice-rule dominated strong proton–proton correlations to be the main physics of the system. Motivated by experiments and the previous studies, the phase diagram in the T – K plane suggests that the qualitative shape of the critical boundary T_c is more closer to a linear behavior for small field strength consistent with the experimental results [41–43], though at large pressure, T_c and T^* does not behave linearly in contrast to experimental results where one finds a complete linear behavior for all ranges of applied pressure. Another aspect that we find in our study is the difference between T_c and T^* which remains constant through out all pressure ranges, which to our opinion is a remarkable success of our study. However, our results indicate a possible second order phase transition in contrast to experiments. This deviation with experiments might be reconciled by considering the inter layer coupling or more complicated couplings to lattice distortions, which are neglected in our model. The temperature dependence of the interaction parameter can not be ruled out as well. The anomalous specific heat peak at low temperature in the ferroelectric phase is due to the formation of cluster of ferroelectric domains. The height of the peak reduces with the increase of system size

suggesting that for small system, the domain size is comparable to the system itself. The fact that the height of this anomalous peak as well as the critical temperature depends on the strength of dipole–dipole interaction which renders the squaric acid system as an interesting system for experimental confirmation of the same.

Another important aspect is the nature of phase diagram in T – K plane which is linear for small and intermediate values of K and for large values of K it becomes elliptical. We think the distinct feature of our results shows that a four-spin interaction at the zeroth order is more realistic. Also in the present model the dependence of degeneracy of ground state manifold is different from the two-spin Hamiltonian. For example, at the zeroth order, four spin interaction includes non-ice rule states as well (all spin up and all spin down in a given plaquette) ice-rule states. The diagonal Ising like interaction reduces the macroscopic ground state degeneracy to be proportional linearly to the system dimension. However for the two body case, the degeneracy is still macroscopic. We believe that this might be the reason that the present study is more closure to the experimental realization.

To summarize, we have studied the finite temperature phase diagram of proton dynamics of squaric acid system. The study offers a unique opportunity to examine the competition between quantum fluctuation and thermal fluctuation and the effect of intricate ground state degeneracy of such system. The model Hamiltonian we considered involves a four-spin interaction which renders the present study an interesting one in view of the successfully solving the model as well as to qualitatively reproduce the experimental findings.

In our endeavor to study such a Hamiltonian (2.1) involving four-spin interaction, we used SSE quantum Monte Carlo involving an improvised version of loop update algorithm which efficiently overcome the problem of ergodic sampling in some parameter regimes. Our theoretical study successfully detected the quantum liquid-like intermediate state before the appearance of conventional para-electric state as we increase the temperature. The ferroelectric state which exist before the liquid like quantum liquid-like state, is characterized by its colossal dependence of T_c with respect to J_2 , the dipole–dipole interaction. In the intermediate liquid-like state, the local correlations governing the ice-rule constraints are still valid to a large extent. While the experimental phase diagram in T – K plane, the phase transition shows a linear behavior for all K , we find the linear behavior for small and intermediate values of K . Thus though our results fall short of full experimental confirmation, still it is quite an improvement in regard to the earlier theoretical study so far. Also the phase transition from the ferroelectric phase to quantum liquid like state is more sharper which reasserts that the model which is considered here is more practical as far as the squaric acid system is concerned. For further improvement of our results, a first-principle calculations would be helpful to establish the correct Hamiltonian as well as fixing the realistic parameters. In addition to this, the inter layer coupling should be considered to fill the gap between the theoretical and experimental studies. This effort is beyond the scope of present study and are kept as a future scope.

Acknowledgments

The authors thank Kedar Damle and Sounak Biswas for fruitful discussions on SSE QMC.

ORCID iDs

Saptarshi Mandal  <https://orcid.org/0000-0001-8261-0483>

References

- [1] Blinc R and Ohys J 1960 *J. Phys. Chem. Solids* **13** 204
- [2] Matsushita E and Matsubara T 1982 *Prog. Theor. Phys.* **67** 1
- [3] Slater J C 1941 *J. Chem. Phys.* **9** 16
- [4] Blinc R 1960 *J. Phys. Chem. Solids* **13** 204
- [5] Samara G A 1971 *Phys. Rev. Lett.* **27** 103
- [6] Peercy P S and Samara G A 1973 *Phys. Rev. B* **8** 2033
- [7] de Gennes P G 1963 *Solid State Commun.* **1** 132
- [8] Bernal J D and Fowler R H 1933 *J. Chem. Phys.* **1** 515
- [9] Samuelsen E J and Semmingsen D 1977 *J. Phys. Chem. Solids* **38** 1275
- [10] Pauling L 1935 *J. Am. Chem. Soc.* **57** 2680
- [11] Moritomo Y, Tokura Y, Takahashi H and Mori N 1991 *Phys. Rev. Lett.* **67** 2041
- [12] Chern C-H and Nagaosa N 2014 *Phys. Rev. Lett.* **112** 247602
- [13] Vijigiri V and Mandal S 2018 *Phys. Rev. B* **98** 224425
- [14] Savit R 1980 *Rev. Mod. Phys.* **52** 453
- [15] Maier H D, Muser H E and Petersson J 1982 *Z. Phys. B* **46** 251
- [16] Reiter G F, Mayers J and Platzman P 2002 *Phys. Rev. Lett.* **89** 135505
- [17] Shannon N, Sikora O, Pollmann F, Penc K and Fulde P 2012 *Phys. Rev. Lett.* **108** 067204
- [18] Shannon N, Misguich G and Penc K 2004 *Phys. Rev. B* **69** 220403
- [19] Ross K A, Savary L, Gaulin B D and Balents L 2011 *Phys. Rev. X* **1** 021002
- [20] Syljuasen O F and Chakravarty S 2006 *Phys. Rev. Lett.* **96** 147004
- [21] Ardonne E, Fendley P and Fradkin E 2004 *Ann. Phys.* **310** 493
- [22] Lines M E and Glass A M 1977 *Principles and Applications of Ferroelectrics and Related Materials* (New York: Oxford University Press)
- [23] Horiuchi S and Tokura Y 2008 *Nat. Mater.* **7** 357
- [24] Deininghaus U 1981 *Z. Phys. B* **45** 71
- [25] Stilck J F and Salinas S R 1981 *J. Chem. Phys.* **75** 1368
- [26] Zinenko V I 1976 *Phys. Status Solidi B* **78** 721
- [27] Matsushita E, Yoshimitsu K and Matsubara T 1980 *Prog. Theor. Phys.* **64** 1176
- [28] Semmingsen D 1973 *Acta Chem. Scand.* **27** 3961
- [29] Chaudhuri B K, Dey P K and Matsuo T 1990 *Phys. Rev. B* **41** 2479
- [30] Sandvik A W 2003 *Phys. Rev. E* **68** 056701
- [31] Swendsen R H and Wang J S 1987 *Phys. Rev. Lett.* **58** 86–8
- [32] Wolff U 1989 *Phys. Rev. Lett.* **62** 361–4
- [33] Liu J, Qi Y, Meng Z Y and Fu L *Phys. Rev. B* **95** 041101(R)
- [34] Huang L and Wang L 2017 *Phys. Rev. B* **95** 035105
- [35] Liu J, Shen H, Qi Y, Meng Z Y and Fu L 2017 *Phys. Rev. B* **95** 241104(R)
- [36] Xu X Y, Qi Y, Liu J, Fu L and Meng Z Y 2017 *Phys. Rev. B* **96** 041119(R)
- [37] Biswas S and Damle K 2018 arXiv:1812.05326
- [38] Sandvik A W 1992 *J. Phys. A: Math. Gen.* **25** 3667
- [39] Ishizuka H, Motome Y, Furukawa N and Suzuki S 2011 *Phys. Rev. B* **84** 064120
- [40] Binder K 1981 *Z. Phys. B* **43** 119
- [41] Barth E, Helwig J, Maier H D, Muser H E and Petersson J 1979 *Z. Phys. B* **34** 393
- [42] Kuhn W, Maier H D and Petersson J 1979 *Solid State Commun.* **32** 249
- [43] Mehring M and Becker J D 1981 *Phys. Rev. Lett.* **47** 366